Evaluation of Whole Atmosphere Community Climate Model simulations of ozone during Arctic winter 2004–2005

M. Brakebusch,[1] C. E. Randall,[1] D. E. Kinnison,[2] S. Tilmes,[2] M. L. Santee,[3] and G. L. Manney[3,4,5]

Received 24 August 2012; revised 17 January 2013; accepted 27 January 2013; published 29 March 2013.

[1] The work presented here evaluates polar stratospheric ozone simulations from the Whole Atmosphere Community Climate Model (WACCM) for the Arctic winter of 2004–2005. We use the Specified Dynamics version of WACCM (SD-WACCM), in which temperatures and winds are nudged to meteorological assimilation analysis results. Model simulations of ozone and related constituents generally compare well to observations from the Earth Observing System Microwave Limb Sounder (MLS). At most times, modeled ozone agrees with MLS data to within ~10%. However, a systematic high bias in ozone in the model of ~18% is found in the lowermost stratosphere in March. We attribute most of this ozone bias to too little heterogeneous processing of halogens late in the winter. We suggest that the model under-predicts $ClONO_2$ early in the winter, which leads to less heterogeneous processing and too little activated chlorine. Model HCl could also be overestimated due to an underestimation of HCl uptake into supercooled ternary solution (STS) particles. In late winter, the model overestimates gas-phase HNO_3, and thus NO_y, which leads to an over-prediction of $ClONO_2$ (under-prediction of activated chlorine). A sensitivity study, in which temperatures for heterogeneous chemistry reactions were reduced by 1.5 K, shows significant improvement of modeled ozone. Chemical ozone loss is inferred from the MLS observations using the pseudo-passive subtraction approach. The inferred ozone loss using this method is in agreement with or less than previous independent results for the Arctic winter of 2004–2005, reaching 1.0 ppmv on average and up to 1.6 ppmv locally in the polar vortex.

Citation: Brakebusch, M., C. E. Randall, D. E. Kinnison, S. Tilmes, M. L. Santee, and G. L. Manney (2013), Evaluation of Whole Atmosphere Community Climate Model simulations of ozone during Arctic winter 2004–2005, *J. Geophys. Res. Atmos.*, *118*, 2673–2688, doi:10.1002/jgrd.50226.

1. Introduction

[2] Understanding the recovery of polar stratospheric ozone (O_3) is important because O_3 shields the Earth's surface from harmful solar radiation and is itself a radiatively active gas. It is expected that the recovery of polar stratospheric O_3 will be influenced by, and influence, global climate change [e.g., *World Meteorological Organization*, 2011; *Akiyoshi et al.*, 2010]. To reliably predict future O_3 variations, it is important to understand the dynamical and chemical processes relevant to ozone loss. Although in general the mechanisms behind polar stratospheric ozone loss are well understood [e.g., *Solomon*, 1999; *Brasseur and Solomon*, 2005], there are still differences in the chemistry modules of state-of-the-art chemistry climate models, differences in the parameterizations and approximations applied, and differences in the dynamical description of the vortex that can lead to significant discrepancies in the representation of polar ozone loss [*Eyring et al.*, 2010, chapter 6]. The overall goal of this study is to assess Whole Atmosphere Community Climate Model (WACCM) [*Eyring et al.*, 2010, chapter 2.4.16 and references therein] simulations of polar stratospheric O_3 by comparing WACCM results to observations from the Earth Observing System Microwave Limb Sounder (EOS MLS, hereafter called MLS) onboard NASA's Aura satellite. The Northern Hemisphere (NH) winter of 2004–2005 is chosen for the model/measurement comparisons since this winter was one of the coldest in recent years, and it has been investigated by numerous authors, as described later in this section [*Jin et al.*, 2006b; *Manney et al.*, 2006; *Rex et al.*, 2006; *von Hobe et al.*, 2006; *Feng et al.*, 2007; *Grooß*

[1]Department of Atmospheric and Oceanic Sciences and Laboratory for Atmospheric and Space Physics, University of Colorado at Boulder, Boulder, Colorado, USA.
[2]Atmospheric Chemistry Division, National Center for Atmospheric Research, Boulder, Colorado, USA.
[3]Jet Propulsion Laboratory, California Institute of Technology, Pasadena, California, USA.
[4]Also at New Mexico Institute of Mining and Technology, Socorro, New Mexico, USA.
[5]Now at NorthWest Research Associates, Socorro, New Mexico, USA.

Corresponding author: M. Brakebusch, Department of Atmospheric and Oceanic Sciences and Laboratory for Atmospheric and Space Physics, University of Colorado at Boulder, Boulder, CO, USA. (brakebusch@colorado.edu)

2169-897X/13/10.1002/jgrd.50226

and Müller, 2007; *Singleton et al*., 2007; *Tsvetkova et al*., 2007; *El Amraoui et al*., 2008; *Jackson and Orsolini*, 2008; *Rösevall et al*., 2008; *Santee et al*., 2008; *Feng et al*., 2011]. This winter thus provides a good test case for evaluating WACCM.

[3] The meteorology of the 2004–2005 Arctic winter is described in detail by *Manney et al*. [2006] and is briefly summarized here. The Arctic winter 2004–2005 was colder than average, but the polar vortex was quite variable in shape and location. The vortex was disturbed by warmings in late December, late January, and February. These caused mixing events across the vortex edge that led to variations in trace gases. Descent was the dominant transport process until late January, when chemical O_3 loss became significant. Throughout February and persisting until the early final warming around 10 March, transport was dominated by mixing events inside the polar vortex and across the polar vortex edge. Intrusions of extra-vortex air into the vortex were evident as the vortex began to break up. More details of the meteorology will be discussed in section 3.3.

[4] Chemistry relevant to O_3 loss during the 2004–2005 Arctic winter is described in detail by *Santee et al*. [2008]. With large areas of the polar vortex being cold enough for PSCs for significant periods of time, substantial growth of PSC particles and subsequent denitrification occurred [*Kleinböhl et al*., 2005; *Dibb et al*., 2006; *Jin et al*., 2006a]. PSCs consisting of supercooled ternary solution (STS) particles and nitric acid trihydrate (NAT) particles were observed [*Blum et al*., 2006], and ice particles were inferred from water vapor observations [*Jiménez et al*., 2006]. The onset of chlorine (Cl) activation was found in MLS observations in late December/early January, with highest ClO enhancements at 490 K after 10 January. Reactive Cl peaked in late January and early February, with 80–90% of total Cl activated.

[5] Quantifying chemical O_3 loss requires identifying the separate contributions of transport and chemistry to observed O_3 changes. Chemical O_3 loss in the Arctic 2004–2005 winter has been quantified using several different techniques. *Manney et al*. [2006] estimated the loss using the polar vortex average descent technique [*Hoppel et al*., 2002], which was also used by *El Amraoui et al*. [2008]. In the vortex average descent technique, differences between the observations and a simulated descended O_3 profile in the polar vortex represent chemical O_3 loss. A similar approach, in which diabatic descent was estimated from a radiation model, was used by *Tsvetkova et al*. [2007] to quantify O_3 loss. *Rex et al*. [2006] used a Lagrangian approach where air parcels were probed along their trajectory by O_3 sondes, and changes in the O_3 mixing ratios were attributed to chemical O_3 loss [e.g., *Rex et al*., 1999]. Tracer correlation techniques [*Michelsen et al*., 1998; *Proffitt et al*., 1992] take advantage of the fact that O_3 chemistry will perturb the relationship between nitrous oxide (N_2O) and O_3 that is established when both act as tracers [e.g., *Tilmes et al*., 2004]. This method was also used by *von Hobe et al*. [2006] to estimate chemical O_3 loss in the Arctic 2004–2005 polar vortex. *Rösevall et al*. [2008] used a modified tracer correlation method to derive chemical O_3 loss. They also calculated O_3 loss applying the passive subtraction technique [originally developed by *Manney et al*., 1995], which is also used here and is described in section 4.1. *Jackson and Orsolini* [2008], *Grooß and Müller* [2007], and *Singleton et al*. [2007] also applied the passive subtraction method. *Jin et al*. [2006b] used a variety of techniques: tracer correlation, artificial tracer correlation [*Esler and Waugh*, 2002], vortex average profile descent [*Manney et al*., 2006], and correlations between potential PSC volume and chemical O_3 loss [*Rex et al*., 2004]. Results of these studies are listed in section 5 along with a comparison to findings from this study.

[6] Section 2 describes the observations from MLS and the simulations from WACCM used for this study. In section 3, we compare WACCM simulations of temperature, polar stratospheric O_3 and related constituents to observations from MLS for the 2004–2005 winter. We quantify chemical ozone loss using the passive subtraction method in section 4. Also shown in section 4 is a temperature sensitivity study for modeled heterogeneous chemistry. Section 5 summarizes the results, compares findings to previous studies, and provides conclusions.

2. Method

[7] The Community Earth System Model version 1.0.3 WACCM component set is a coupled chemistry climate model developed at the National Center for Atmospheric Research, originally based on the software framework of the Community Atmosphere Model (CAM) [*Collins et al*., 2006]. The WACCM chemistry module is taken from the Model for OZone And Related chemical Tracers (MOZART) [*Brasseur et al*., 1998; *Hauglustaine et al*., 1998; *Horowitz et al*., 2003; *Kinnison et al*., 2007; *Emmons et al*., 2010] but is extended to include 122 species [*Lamarque et al*., 2012]. The upper atmosphere module is taken from the Thermosphere-Ionosphere-Mesosphere Electrodynamics General Circulation Model (TIME-GCM) [*Roble and Ridley*, 1987]. The specified dynamics version of WACCM, SD-WACCM, is a modified version of WACCM in which the meteorology is constrained to match observations to within a user-defined tolerance [*Lamarque et al*., 2012; *Kunz et al*., 2011]. Thus, whereas WACCM is a free-running general circulation model, SD-WACCM is nudged every 30 min time step with horizontal winds, temperatures, and surface pressure from a meteorological assimilation analysis to prevent divergence from real dynamical conditions. Additionally, SD-WACCM is forced with surface wind stress and sensible as well as latent surface heat flux.

[8] The simulations described below use SD-WACCM with a horizontal resolution of $1.9^\circ \times 2.5^\circ$ (latitude $\times$ longitude) and a vertical hybrid sigma-pressure coordinate with 88 levels that range in resolution from about 0.5 to 4 km and cover an altitude range from the surface to about 145 km. Vertical resolution in the lower stratosphere, the region of primary interest here, is ~1 km. Winds, temperature, surface pressure, surface wind stress, and heat fluxes used here are from the Goddard Earth Observing System 5 (GEOS5) analysis [*Reinecker et al*., 2008]. This analysis product has a 6 h time resolution, which is interpolated by the model to the finer 30 min time resolution required. The nudging coefficient is 0.01, i.e., the winds, temperature, and surface pressure are defined by a linear combination of 1% from GEOS5 and 99% from the model. This nudging scheme is used below

50 km, while above 60 km the model is fully interactive; at altitudes from 50 to 60 km a linear transition occurs from 1% to 0% nudging. Although the nudging coefficient seems small in magnitude, it is compounded at each time step. Thus after an initial spin-up time period (see below), the SD-WACCM winds and temperatures are very similar to GEOS5 and require only a small amount of nudging to remain so. More specifically, the mean differences (SD-WACCM minus GEOS5 $\pm$ one standard deviation (σ) over the winter) are -0.16 ± 0.77 K for temperature, -0.08 ± 1.83 m/s for zonal wind, and -0.01 ± 1.9 m/s for meridional wind. Vertical transport is derived by SD-WACCM following a transport scheme developed by *Lin and Rood* [1996] and *Lin* [2004]. Gravity waves are parameterized [*Richter et al*., 2010] while planetary waves are resolved. In the model, wind stress and heat fluxes are forced (not nudged) to exactly match GEOS5. SD-WACCM can therefore simulate the atmosphere up to about the stratopause with specific dynamics representing a particular season, enabling direct comparison to tropospheric and stratospheric observations. In contrast, a climatological WACCM simulation will be representative of an average season, but will not replicate crucial characteristics of a specific season.

[9] The SD-WACCM simulations employed here correspond to the time period from 1 December 2004 to 31 March 2005. For these simulations the model had a spin-up time from 1980 to the end of 2003 in fully interactive mode, i.e., free-running WACCM, without specified dynamics, was used for the initial spin-up. On 1 January 2004, the model was switched to SD-WACCM; the 11 month period from January to December 2004 was a sufficient spin-up time for the nudging, as mentioned above. In order to evaluate SD-WACCM via comparison of modeled to observed species, initial conditions in the model are set equal to the observations used for comparison (MLS in this case, as explained below). This is necessary in order to accurately interpret deviations between the model results and observations. Thus, within the accuracy and precision of the observations, these deviations can be attributed to the model. At the same time the simulations can only be compared to data from the instrument used for the initialization since biases between instruments exist. For a model simulation without this initialization (not shown), the same conclusions were drawn qualitatively but a quantification of model/instrument differences was not possible. The initialization date chosen in this study is 1 December 2004, which is before the first halogen-catalyzed lower stratospheric O_3 loss occurs. Because MLS provides near global observations, it is used for the initialization, as described in more detail below. This allows for initialization of gas-phase O_3, N_2O, nitric acid (HNO_3), hydrochloric acid (HCl), and water vapor (H_2O).

[10] In addition to data from other instruments, well-validated limb emission data since August 2004 are available from the MLS instrument [*Livesey et al*., 2011], with nearly global coverage and a vertical resolution of 3–10 km, which varies with constituent and altitude. For this study we use version 3.3 Level 2 data. For the vertical range of interest for this study, 17–100 hPa, accuracy (precision) is on the order of $\pm$0.1 ppbv to $\pm$0.05 ppbv ($\pm$0.1 ppbv) for ClO, $\pm$4% to $\pm$8% ($\pm$6% to $\pm$15%) for H_2O, 0.1 ppbv to 0.2 ppbv (0.2 ppbv to 0.3 ppbv) for HCl, $\pm$0.5 ppbv to $\pm$2 ppbv ($\pm$0.7 ppbv) for HNO_3, 13 ppbv to 70 ppbv (13 ppbv to 24 ppbv) for N_2O, 0.05 ppmv to 0.25 ppmv (0.04 ppmv to 0.1 ppmv) for O_3, and -2 K to +1 K ($\pm$0.6 to $\pm$0.8K) for T [*Livesey et al*., 2011]. The low bias correction suggested by *Livesey et al*. [2011] for MLS ClO version 3.3 was applied to all ClO observations used in this study. For the NH lower stratosphere polar vortex region, the bias correction is on the order of 7–160 pptv and strongly depends on latitude and pressure.

[11] For model initialization, a regularly gridded form of the MLS Level 2 data is required. The grid for one day of MLS observations is created by applying to the observations, separately for each pressure level, a spatial Delaunay Triangulation [*Knuth*, 1992 and references therein]. Spatial noise is reduced by applying a distance-weighted smoothing. As an example, Figure 1 shows one day of NH MLS O_3 measurements on the 100 hPa pressure level (potential temperature ~420 K, or ~16 km), depicted as symbols that are color-coded according to the observed O_3 volume mixing ratio. The color contours show the same data after gridding to a regular $1.9° \times 2.5°$ field. The largest interpolations occur between 30°N and 30°S, where zonal distances in the MLS sampling are ~14°. Data gaps at latitudes poleward of 82° are filled by interpolating across the poles. Near-global coverage of MLS observations on any level is required to create the above described gridded product. Data for the lowest and highest retrieved levels of MLS observations may not fulfill this criterion; hence the altitude range for each species used for the gridded product may be reduced from the published valid range.

[12] By default WACCM is initialized with all atmospheric constituents from a previously completed climatological simulation. For the initialization in this study, each profile of H_2O, HCl, HNO_3, N_2O, and O_3 from the default initialization is replaced globally with the gridded MLS data described above, within the altitude range over which both the MLS data and the gridding procedure are valid. At the upper and lower altitude limits of this range, the profiles smoothly transition back to the climatological WACCM profiles. Table 1 lists the altitude ranges for each constituent

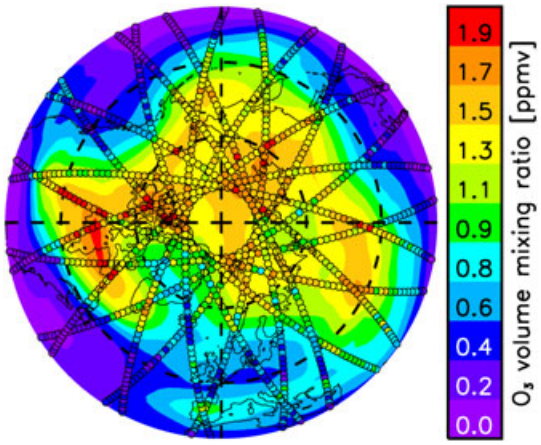

Figure 1. Contour map of gridded MLS O_3 data at 100 hPa on 1 December 2004. Colored dots represent MLS measurements from which the gridded data was produced (see text).

Table 1. SD-WACCM Initialization Altitudes

	SD-WACCM	MLS	SD-WACCM
O_3	≥164 hPa (≤350 K)	101–2.95 hPa (400–1350 K)	≤0.91 hPa (≥2000 K)
N_2O	≥101 hPa (≤400 K)	43.9–2.95 hPa (550–1350 K)	≤0.91 hPa (≥2000 K)
H_2O	≥164 hPa (≤350 K)	101–0.06 hPa (400–3550 K)	≤0.015 hPa (≥5050 K)
HNO_3	≥101 hPa (≤400 K)	61.5–12.5 hPa (475–825 K)	≤4.56 hPa (≥1150 K)
HCl	≥101 hPa (≤400 K)	61.5–2.95 hPa (475–1350 K)	≤0.91 hPa (≥2000 K)

over which the different initializations are used. For example, the initialization profiles of O_3 are equal to MLS O_3 between 101 hPa and 2.95 hPa, and to the 1 December WACCM profiles at pressure levels greater than 164 hPa or smaller than 0.91 hPa. Between 164 hPa and 101 hPa (2.95 hPa and 0.91 hPa), a linear transition is made across two (four) pressure levels. When this technique was applied to HCl, it introduced unrealistic structure in the HCl profiles at altitudes above 0.91 hPa; thus for HCl only, WACCM mixing ratios at altitudes above 0.91 hPa are scaled to MLS mixing ratios in the transition region. For pressure levels greater than 44 hPa, the slope of the N_2O volume mixing ratio profile with respect to altitude steepens sharply, which causes the initialization of N_2O to become particularly sensitive to the number of transition levels. Thus for pressure levels greater than 44 hPa, N_2O is initialized with the climatological WACCM profiles.

[13] In order to improve WACCM's capability to accurately simulate polar O_3 and related constituents, several modifications to the representation of heterogeneous chemistry were included. In this paragraph, we describe the default WACCM without improvements first and then introduce the modifications. In its standard configuration, the WACCM heterogeneous module is based on an equilibrium approach and the observed sulfate surface area density of a volcanically clean atmosphere is used [*Kinnison et al*., 2007]. In the equilibrium approach, the total available HNO_3 is partitioned between STS and NAT particles based on temperature and composition factors. This approach allows NAT to form at ~195 K, several degrees warmer than the temperature at which STS becomes important in taking up HNO_3. Therefore, in early winter, NAT particles are the primary HNO_3 containing particles and subsequent denitrification rapidly occurs. Based on observational evidence, this approach was modified for the current work [Wegner, T., D. E. Kinnison, R. R. Garcia, S. Madronich, S. Solomon, and M. von Hobe (2012), Polar Stratospheric Clouds in SD-WACCM4, manuscript in preparation, hereafter called *Wegner et al*., 2012a]. In the new approach, the partitioning of total available HNO_3 is forced to not exceed 80% uptake into STS and 20% into NAT. Further, the NAT particle density is reduced to 10^{-3} cm^{-3}, which again is based on observational evidence [*Pitts et al*., 2009]. These two modifications have greatly improved the absolute and temporal agreement of model gas-phase HNO_3 as observed by MLS [*Wegner et al*., 2012a]. In terms of chlorine activation, heterogeneous chemistry reactions on STS particles have been found to be the dominant source of reactive chlorine [*Wegner et al*., 2012; *Drdla and Müller*, 2012]. A third modification, HCl condensation into STS, has also been added. This parameterization is based on laboratory measurements and is highly dependent on temperature and H_2O vapor abundance [*Lowe and MacKenzie*, 2008]. This process allows gas-phase HCl to be absorbed into the particle. The soluble HCl will only be activated if there is enough chlorine nitrate ($ClONO_2$), HOCl, or HOBr available to heterogeneously react [Wegner, T., D. E. Kinnison, R. R. Garcia, S. Madronich, S. Solomon, and M. von Hobe (2012), Chlorine Partitioning in the Antarctic Stratosphere: Implications of HCl uptake into STS, manuscript in preparation, hereafter called *Wegner et al*., 2012b].

[14] In addition, the total inorganic bromine abundance in the model was increased globally on 1 December 2004 by a factor of 1.5 (from ~16 pptv to ~24 pptv). This increase in total inorganic bromine was applied as a surrogate to represent very short-lived organic bromine species not included in the WACCM chemical mechanism. See *Salawitch et al*. [2010], *World Meteorological Organization* [2011], and *Tilmes et al*. [2012] for more details on very short-lived halogen abundances in the atmosphere. The photolysis approach used in WACCM is based on a lookup table described by *Kinnison et al*. [2007] and evaluated by *Eyring et al*. [2010].

3. Model/Measurement Comparisons

[15] This section shows comparisons between SD-WACCM simulations and measurements of temperature, O_3, and chemical constituents that serve as diagnostics of transport and chemistry. The area of interest is the lower polar stratosphere, i.e., the potential temperature range from 400 (~18 km or ~100 hPa) to 700 K (~28 km or ~17 hPa). For the comparisons, SD-WACCM is sampled at MLS observation positions and times, within the model accuracy, which is $\pm 1.25°$ longitude, $\pm 0.9°$ latitude, and ± 15 min, i.e. the closest profile is chosen and no interpolation is done. Subsequently, all SD-WACCM profiles of any species shown in this study are modified by applying the averaging kernels from the MLS retrieval as described in detail by *Livesey et al*. [2011]. All observations inside the polar vortex are averaged to a single, daily profile unless stated otherwise. The polar vortex is defined by scaled potential vorticity (sPV) [*Dunkerton and Delisi*, 1986] values greater than 1.4×10^{-4} s^{-1}. In contrast to Ertel's potential vorticity, sPV does not depend on altitude but retains all spatial variations as well as conservation properties. Thus a single threshold as a polar vortex edge criterion can be applied for the entire altitude range in this study. Because of the relatively dense MLS measurement sampling at high latitudes, the polar vortex is well sampled equatorward of 82°N. That is, the MLS measurement locations generally range from the inner vortex core out to the edge and beyond. Therefore, averaging observations or model output at MLS observation positions within the vortex is typically representative of an average full range of conditions in the polar vortex. For polar map projection figures, observations and simulations from that particular day are gridded in the same way as described for the model initialization.

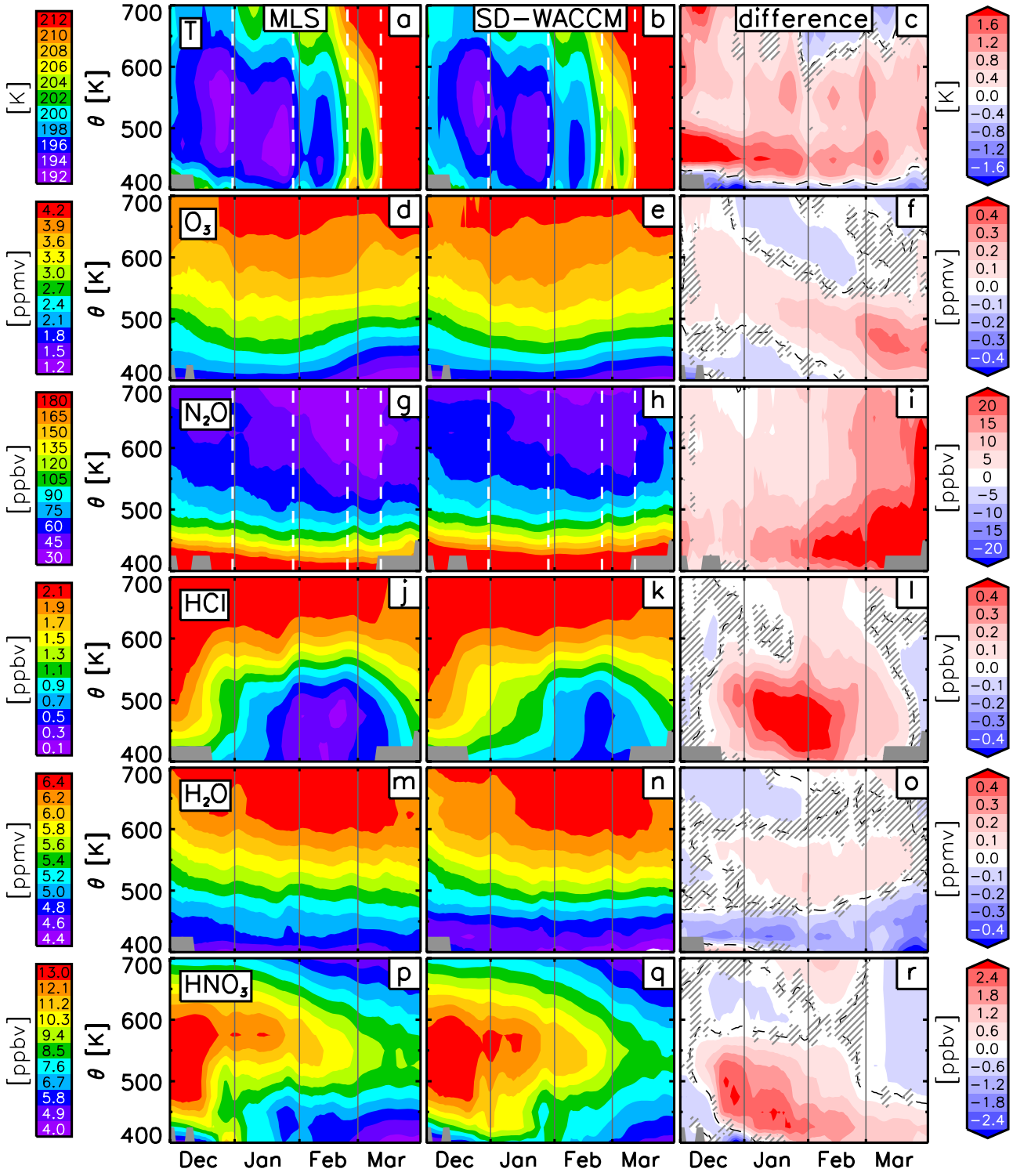

Figure 2. Evolution of vortex averaged MLS observations (left), SD-WACCM (center), and their difference (right) for temperature, O_3, N_2O, HCl, H_2O, and HNO_3 (top to bottom). Differences are calculated as (SD-WACCM – MLS). Gray areas denote potential temperatures where data were either missing or acquired only outside the polar vortex. White dashed lines indicate warming events mentioned in section 3.2. Hatched areas in right column indicate differences that are not statistically significant at the 95% confidence level. Black dashed lines denote the zero difference contour.

[16] Comparison results are summarized in Figure 2. A 7-day weighted running average is applied in each panel to cover temporal gaps in the MLS observations. The statistical significance of the model/measurement comparisons is defined by the Wilcoxon signed-rank test [*Wilcoxon*, 1945; *Wilks*, 2006] using the distributions of values within the polar vortex from SD-WACCM and MLS for each day and isentropic surface individually. Thus, the statistical significance indicates whether mean differences between the model and measurements are significant relative to variability within the vortex. The Wilcoxon signed-rank test was chosen here since the underlying distributions tested negative for normality; thus Student's *t*-test does not apply [*Dowdy et al.*, 2004]. Differences between SD-WACCM and MLS that are statistically insignificant with a confidence of 95% are shaded in column 3 of Figure 2.

3.1. Temperature

[17] SD-WACCM is nudged with GEOS5 temperatures, so lower stratospheric SD-WACCM temperatures differ from GEOS5 temperatures only insignificantly (not shown). MLS temperatures are shown in Figure 2a, SD-WACCM (equivalently, GEOS5) temperatures are shown in Figure 2b, and the differences between the two are shown in Figure 2c. Morphologically the temperatures are quite similar, and differences are usually less than ± 2 K. At polar latitudes and between 100 hPa and 17 hPa, the validation of MLS version 3.3 temperature shows differences (GEOS5 minus MLS) of -0.5 ± 0.3 K to $+1.5 \pm 0.6$ K [*Livesey et al.*, 2011; *Schwartz et al.*, 2008]. Although small, the impact of these temperature differences on heterogeneous chemistry is significant; this is discussed in section 4.2. Here the evolution of simulated and observed temperature is discussed in the context of dynamics only. Planetary wave activity causes deceleration of the zonal wind and thus a warming below the forcing region [*Shepherd*, 2000]. Such temperature increases are evident throughout the entire potential temperature range of 400–700 K in late December through early January, late January, in the second half of February through early March, and during the final warming around 10 March. All of these warmings are equally pronounced in the observations and SD-WACCM. The largest statistically significant temperature differences occur in December and January below the 500 K isentropic surface, with SD-WACCM overestimating temperatures by up to 3 K relative to MLS. In general GEOS5 and thus SD-WACCM temperatures are higher than MLS temperatures, a point that is further discussed in section 4.2.

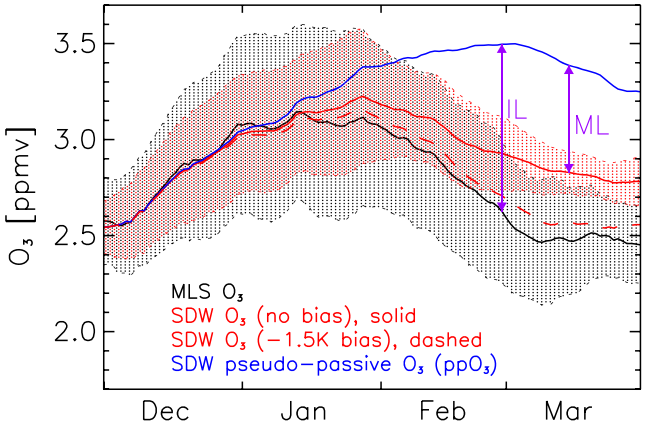

Figure 3. Evolution of vortex averaged MLS O_3 (black), SD-WACCM O_3 (red), and SD-WACCM pseudo-passive ozone (ppO_3, blue) at 475 K. Here, inferred loss (IL, purple) is the difference between MLS O_3 (black) and SD-WACCM ppO_3 (blue); modeled loss (ML, purple) is the difference between SD-WACCM O_3 (red) and SD-WACCM ppO_3 (blue). The black (red) shaded area is MLS (SD-WACCM) O_3 vortex average $\pm$ one standard deviation (σ) of the data used for the vortex average. Also shown is the evolution of vortex averaged SD-WACCM O_3 with a -1.5 K bias for heterogeneous chemistry (dashed red, see text).

3.2. Ozone

[18] The evolution of NH polar vortex O_3 during the winter of 2004–2005 from MLS and SD-WACCM is shown in Figures 2d and 2e. The overall morphology of O_3 as simulated by SD-WACCM is in good agreement with that observed by MLS. Figure 2f shows that differences never exceed 0.35 ppmv; this corresponds to differences that are generally less than 15%. Small (mostly statistically insignificant) differences on day 1 of the simulation are caused in part by an inexact match between the actual MLS data and the gridded product used to initialize SD-WACCM. The inexact match on day 1 is due to the 7-day running average as well as the spatial smoothing explained in section 2.

[19] Figure 3 illustrates the O_3 variability within the vortex in more detail for the 475 K potential temperature level. Here the solid red (black) curve represents vortex mean SD-WACCM (MLS) O_3 mixing ratios during the 2004–2005 winter; shaded areas show the vortex mean $\pm 1\sigma$. On any given day the number of MLS profiles averaged is between ~100 and ~500. The standard deviation shown in Figure 3 reflects spatial variations inside the polar vortex. The model and measurements both show increasing O_3 mixing ratios until late January, followed by decreases throughout February and early March. SD-WACCM mixing ratios begin to diverge from MLS mixing ratios in late January, with differences reaching about 0.35 ppmv (~13%) by mid March. Part of this deviation is caused by the small high bias of ~0.1 ppmv seen in Figure 2f above 500 K in early December, which descends throughout the season. We attribute the December high bias to a deficiency in the initialization procedure for O_3. The remainder of the difference between MLS and SD-WACCM seen in Figure 2f in March below 500 K is attributed to errors in chemistry as explained in section 3.4. The model shows considerably less variation inside the vortex than MLS, as indicated by the narrower shaded area in the model in Figure 3; but the 1σ distribution in the model strongly overlaps the 1σ distribution in the observations until early March. Based on the underlying distributions producing the averages, the Wilcoxon signed-rank test shows that differences between vortex-averaged MLS and SD-WACCM O_3 mixing ratios are statistically significant after late January. Thus, Figures 2d–2f and 3 indicate that SD-WACCM in general overestimates O_3 during the Arctic 2004–2005 winter in the primary O_3 loss region inside the polar vortex below ~525 K. To investigate the reasons behind this overestimate, diagnostics of transport and chemistry are evaluated in the following sections.

3.3. Transport

[20] Vertical transport and mixing in SD-WACCM are investigated by comparing modeled N_2O to MLS measurements. N_2O has a very long lifetime in the lower stratosphere, and is thus a good tracer of transport [*Loewenstein et al.*, 1990]. Figures 2g and 2h show the observed and modeled evolution of vortex average N_2O. As for O_3, the overall morphology of SD-WACCM N_2O is similar to that observed by MLS. Contours at altitudes below about 600 K generally slope downward throughout most of December and January, indicative of diabatic descent inside the vortex. In February the model and measurement contours in this altitude range flatten; they rise toward the end of February, although not as much in the observations as in the model. This is consistent with descent being the dominant transport mechanism in December and January, with mixing becoming more important in February, as discussed by *Manney et al.* [2006]. As also noted by *Manney et al.* [2006], rapid increases in the N_2O mixing ratios after early March indicate the beginning of the vortex breakup.

[21] There are, however, significant differences in the details of the MLS and SD-WACCM comparisons. In particular, SD-WACCM mixing ratios vary more smoothly than observed; for instance, there are smaller deviations during apparent mixing and warming events (indicated by the white dashed lines in Figure 2). At the time of the final warming around 10 March [*Manney et al.*, 2006], MLS N_2O mixing ratios indicate substantial mixing. SD-WACCM mixing ratios of N_2O show less pronounced changes associated with the warming events. Throughout March modeled N_2O mixing ratios increase gradually and relatively smoothly. The final warming is captured appropriately in the simulation, as expected since the meteorology is nudged to GEOS5 data.

[22] Differences between MLS and SD-WACCM N_2O are quantified in Figure 2i. On 1 December differences are below about +10% (SD-WACCM > MLS). Differences on this date reflect deficiencies in the initialization. As shown in Table 1, SD-WACCM is not initialized with MLS data below 550 K, which explains the overestimate below 500 K. The overestimate at higher altitudes likely results from discrepancies that arise from the initialization procedure. Because of these initial disagreements, differences between MLS and SD-WACCM N_2O mixing ratios are interpreted here in a relative sense, focusing on their temporal evolution, not absolute values.

[23] Figure 2i shows increasingly positive N_2O differences (SD-WACCM > MLS) in late February and early March in particular. Over the course of the season descent is gradually replaced by isentropic mixing as the dominant transport process [*Manney et al.*, 2006] and thus becomes less important for controlling constituent distributions. The most likely explanation for these positive differences, therefore, is errors in the SD-WACCM specification of isentropic mixing. At the altitudes shown here, N_2O mixing ratios are lower inside the vortex than outside. Thus an overestimate of N_2O mixing ratios inside the vortex would be consistent with too much SD-WACCM mixing across the vortex edge.

[24] That SD-WACCM overestimates mixing across the vortex edge is supported by Figure 4, which shows N_2O profiles versus equivalent latitude in the descent-dominated early season (5 December, first column), in the mixing-dominated late season (10 March, third column), and in between (20 January, second column). Equivalent analyses are shown for MLS (top row) and SD-WACCM (bottom row). Changes in N_2O that occurred in the first half of the season are shown by the differences plotted in Figure 4d (Figure 4i) for MLS (SD-WACCM). These differences indicate strong descent, as shown by a decrease in volume mixing ratio inside the polar vortex. The increase outside the polar vortex is caused by extra-vortex advection or mixing

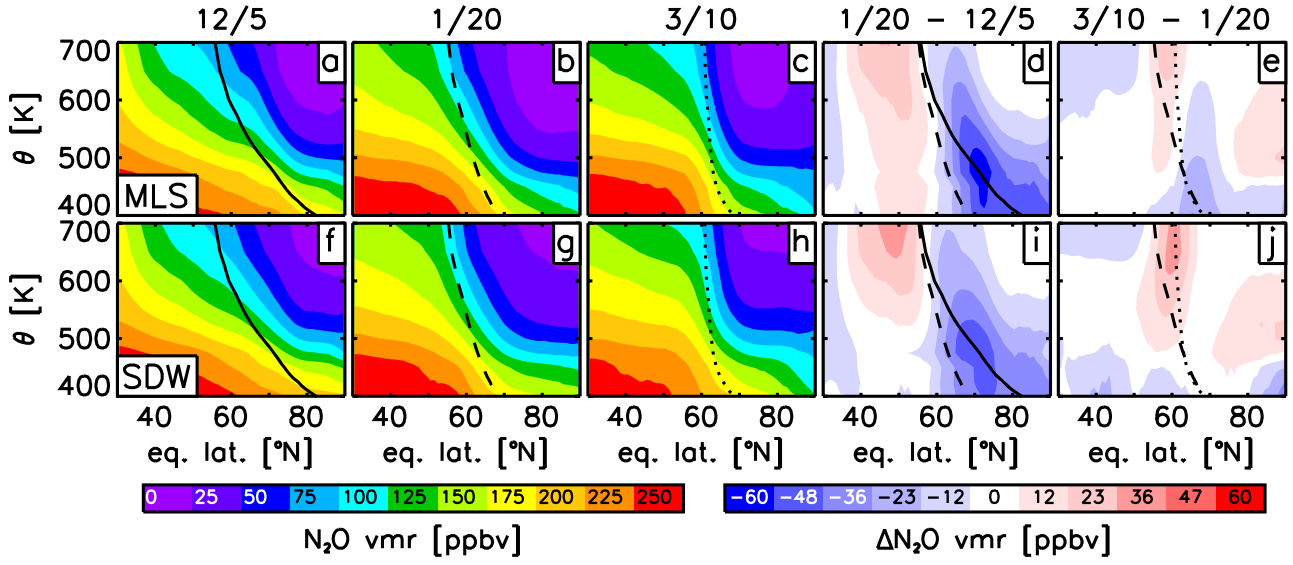

Figure 4. Distribution of N_2O from MLS (top) and SD-WACCM (bottom) versus equivalent latitude and potential temperature for the dates shown above each column. Superimposed in black is the polar vortex edge as a $1.4\times10^{-4}s^{-1}$ sPV line contour (line style coded by date). Panel d (i) shows the 20 January minus 5 December differences for MLS (SD-WACCM). Panel e (j) shows the analogous differences for 10 March minus 20 January.

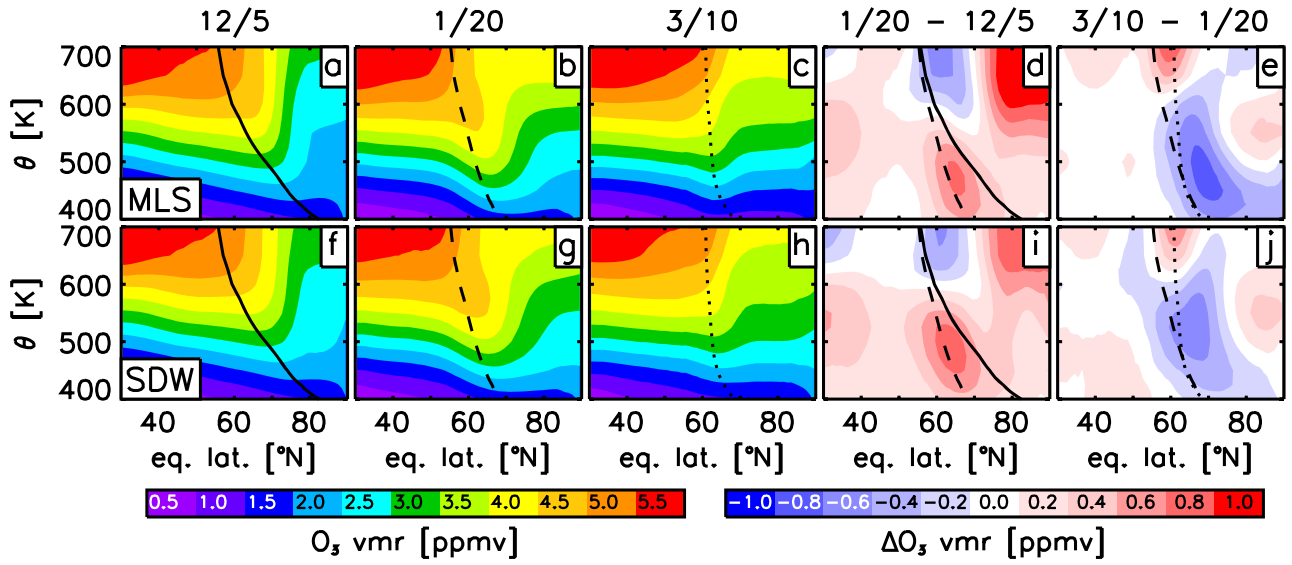

Figure 5. Same as Figure 4, but for O_3.

(see below). The N_2O plots for MLS and SD-WACCM on 5 December and 20 January are very similar in character, so we conclude that descent is fairly well simulated by the model in the first half of the season. Changes in N_2O that occurred in the second half of the season, shown in Figure 4e (Figure 4j) for MLS (SD-WACCM), are more complex with respect to different zones inside the polar vortex [*Manney et al.*, 2006]: At the vortex edge, cross-edge mixing is dominant above 550 K, as indicated by the N_2O increase over time; below 550 K descent is the dominant transport, as in the first half of winter. Inside the vortex above ~450 K, mixing becomes more dominant towards the core region of the polar vortex, as indicated by an increase in N_2O. SD-WACCM captures the overall behavior throughout the vortex, but shows a high bias in the N_2O change near the vortex edge (see Figure 4j). This indicates an overestimate in mixing across the vortex edge in SD-WACCM. To support this finding, Figure 5 shows the same panels as Figure 4 but for O_3. Below 500 K in late winter in particular, the O_3 gradient across the vortex edge is small compared to N_2O, i.e., effects of mixing across the vortex edge will be smaller than effects of descent, in contrast to N_2O. In fact, in the latter half of the winter the O_3 difference in Figures 5e and 5j agree well with each other, emphasizing that descent is correctly simulated. Throughout the winter, a small cross-edge gradient exists above 500 K that is captured well by SD-WACCM. Thus, isentropic mixing results in a weak isentropic dipole structure, with declining O_3 just outside the vortex edge, and increasing O_3 just inside the edge. Such a weak dipole structure is evident above 600 K in Figure 5j, but not in Figure 5e. From both Figures 4 and 5, we thus conclude that SD-WACCM is overestimating mixing across the polar vortex edge and within the polar vortex at all

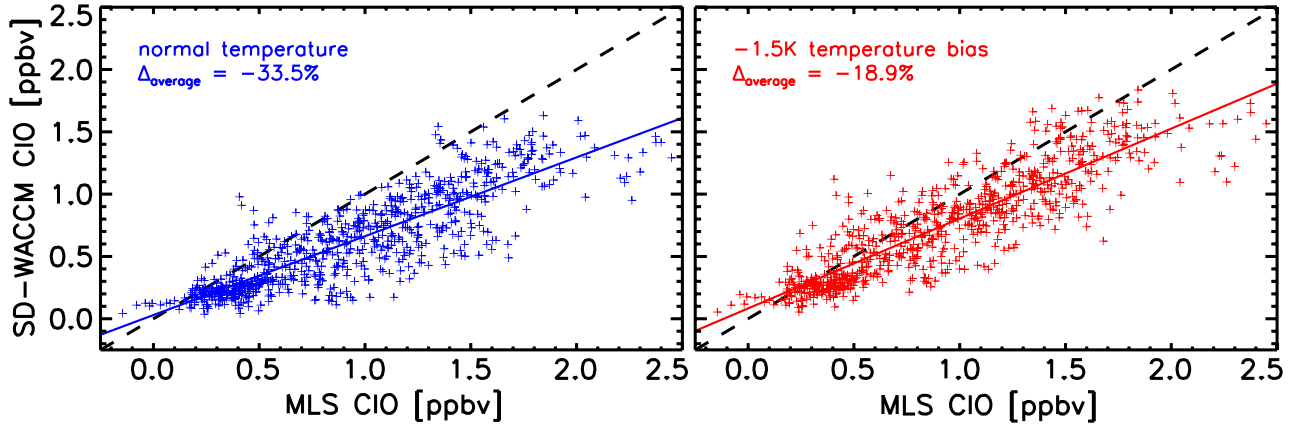

Figure 6. Scatter plot of SD-WACCM ClO versus MLS ClO (blue crosses) on 2 February 2005 between 400 K and 500 K inside the polar vortex. Only daytime values are shown here, identified by a solar zenith angle of less than 90°. The dashed black line shows the ideal 1:1 relation. Also shown is the scatter plot of ClO for the SD-WACCM simulation with a −1.5 K temperature bias for heterogeneous chemistry vs. MLS (red crosses). Linear regressions are shown as solid lines of the same color as the data on which they are based. These regressions only serve as a guide to the eye and were not used for any quantification.

isentropic levels between 400 and 700 K. With regard to Figures 2g–2h, we confirm the overestimate in isentropic cross-edge mixing in the latter half of the season; at the same time there is no clear indication for significant errors in descent.

[25] The O_3 mixing ratios near the edge of the vortex are higher than those inside at altitudes between 400 and 700 K (not shown); thus too much mixing of air across the vortex edge and from the vortex edge into the vortex core in SD-WACCM would lead to a high bias in O_3, consistent with Figure 2f. In conclusion, SD-WACCM captures the general morphology of N_2O, but shows stronger mixing across the vortex edge and throughout the vortex in February and early March in particular. This contributes to an overestimate in the simulated O_3 mixing ratios inside the vortex.

3.4. Halogen Chemistry

[26] In the Arctic winter/spring lower stratosphere, Cl is important for catalytic O_3 destruction [e.g., *Brasseur and Solomon*, 2005]. Chlorine is present in the atmosphere either in the form of inactive, reservoir species HCl and $ClONO_2$, or in the form of reactive species chlorine monoxide (ClO), Cl, ClO dimer (Cl_2O_2), and hypochlorous acid (HOCl). Of these constituents, the MLS instrument measures HOCl, HCl and ClO.

[27] Figure 6 shows that during daytime SD-WACCM ClO is biased low relative to MLS by ~34% on average. If indicative of an underestimate in total reactive chlorine, this would be consistent with an overestimate of O_3 (underestimate of O_3 loss). Fully assessing the SD-WACCM treatment of reactive chlorine partitioning requires observations of Cl and Cl_2O_2 in the vortex throughout the winter, but such observations are not available. We thus cannot infer from Figure 6 errors in total reactive chlorine.

[28] Figures 2j and 2k show that qualitatively, SD-WACCM and MLS HCl compare reasonably well. Both MLS and SD-WACCM show mixing ratios below 550 K that decline from December into February, and then increase throughout March. The decline is steeper in MLS than in SD-WACCM, however, resulting in the high bias in SD-WACCM mixing ratios evident in Figure 2l in December–February below about 550 K. As an example, at 450 K MLS shows a decline in HCl of ~94%, whereas SD-WACCM shows a decline of ~69%. By late February, therefore, HCl mixing ratios at 450 K in SD-WACCM are higher than those measured by MLS by more than 50%. We attribute the overestimate below 550 K to errors in chemistry, as described in the next two paragraphs.

[29] The overall decline that is observed in HCl from January to February is caused primarily by heterogeneous processing of HCl. Based on observations from both MLS and the Atmospheric Chemistry Experiment Fourier Transform Spectrometer (ACE-FTS), *Santee et al.* [2008] found that before the onset of Cl activation, HCl at 490 K in the 2004–2005 Arctic winter vortex represented ~75% of total Cl (Cl_y). Heterogeneous processing led to a decline in HCl so that by late January it represented only ~10% of Cl_y. That HCl in SD-WACCM declines less than in the observations is thus consistent with too little heterogeneous processing in SD-WACCM, which would lead to an underestimate of Cl activation. This might explain part of the overestimate in O_3 that is evident in Figure 2f, since an underestimate of Cl activation would lead to less chemical loss.

[30] A possible factor contributing to the overestimate of HCl by SD-WACCM is an error in Cl reservoir partitioning. Studies have shown that the $ClONO_2$ abundance entering winter is rapidly converted to active chlorine by heterogeneous reactions on STS (and to a lesser extent NAT) by the reactions of $ClONO_2$ with HCl and H_2O [*Portmann et al.*, 1996]. Once the pre-winter $ClONO_2$ is depleted, additional HCl will not be significantly depleted until later in the winter, when photolytic processes reform $ClONO_2$. In this work, pre-winter $ClONO_2$ is not initialized with observations due to scarcity of data on 1 December 2004. There is some indication that the model $ClONO_2$ is biased low (~0.2–0.4 ppbv) in early winter, below 500 K, relative to ACE-FTS observations (not shown). However, the scarcity of $ClONO_2$ data limits this conclusion. The possible low bias in model $ClONO_2$ is not yet understood, but is most likely related to the uncertainty in the $ClONO_2$ gas-phase reaction kinetics, along with possible errors in transport that may lead to an underestimate of pre-winter abundances of inorganic chlorine and inorganic nitrogen. All other things being equal, such an underestimate will lead to too little chlorine activation, and thus too much O_3 (too little O_3 loss), consistent with the results in Figure 2.

[31] As mentioned previously, this version of SD-WACCM includes a parameterization of HCl solubility in STS [*Lowe and MacKenzie*, 2008; *Wegner et al.*, 2012b]. This parameterization is highly dependent on the local water vapor abundance and temperature. *Wegner et al.* [2012b] have shown that a temperature sensitivity of ±1 K centered at 188 K, with a H_2O abundance of 4.5 ppmv, will change the fraction of HCl in the solution phase to the gas-phase from 25% (−1 K) to 0% (+1 K). In addition, assuming the atmospheric temperature is 188 K, the sensitivity of a ±0.5 ppmv H_2O abundance centered at 4.5 ppmv will change this same

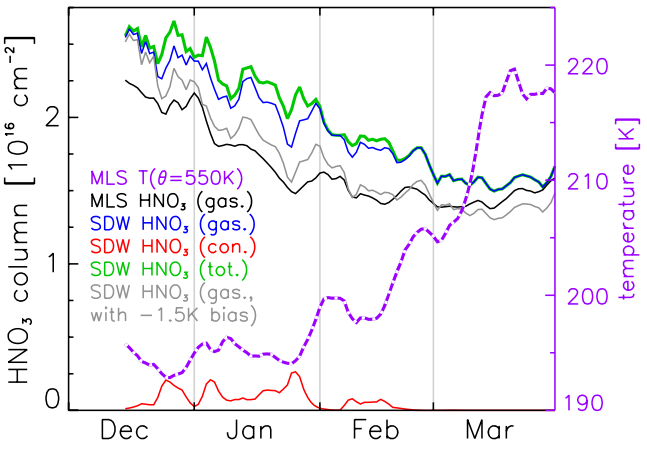

Figure 7. Partial columns (400–700 K) of polar vortex averaged gas-phase HNO_3 from MLS (black) and SD-WACCM (blue). Also shown is modeled condensed-phase HNO_3 (red) and total HNO_3 (green). Note that the sum of the condensed phase HNO_3 and the gas phase HNO_3 is exactly the total HNO_3. MLS temperature at 550 K is superimposed (dashed purple) following the right ordinate. Also shown is SD-WACCM gas-phase HNO_3 with a −1.5 K temperature bias for heterogeneous chemistry (gray). A 7-day running average is applied to all data shown.

fraction from 20% (+0.5 ppmv) to 0% (−0.5 ppmv). Therefore, a high bias in temperature or a low bias in H_2O vapor will shift the HCl equilibrium from the solution to the gas-phase, thus contributing to the overestimate of modeled HCl. Modeled HCl condensation in this winter does not exceed a polar vortex average of 6 pptv in late January below 500 K (not shown), which corresponds to a maximum of ~0.5% of total HCl in the condensed phase.

3.5. PSC Formation

[32] The ratio between inactive and reactive Cl is determined in part by the polar stratospheric cloud (PSC) surface area, since heterogeneous chemistry on the surfaces of primarily STS particles converts inactive Cl to the photoreactive intermediate Cl_2; per convention, we refer to this process as heterogeneous chlorine activation. Subsequent photolysis of Cl_2 then provides Cl for the catalytic O_3 destruction cycles [*Solomon*, 1999]. PSC particles in general are formed by uptake of H_2O and HNO_3, which can lead to permanent dehydration and denitrification if the PSC particles freeze and grow large enough to sediment. Errors in simulating H_2O or HNO_3 can thus indicate errors in simulating the PSC surface area density (SAD), which would then lead to errors in Cl activation and O_3 loss if SAD was the rate limiting property. Thus, comparisons of MLS and SD-WACCM H_2O and HNO_3 can be useful for probing errors in the simulated partitioning between reservoir and active Cl.

[33] Gas-phase H_2O from MLS and SD-WACCM, shown in Figures 2m–2o, compare well; but there is a small (<7%) low bias in the model below 475 K and a small (<3%) high bias above 475 K in December through February. It is possible that the low bias indicates that SD-WACCM slightly overestimates the uptake of H_2O by PSCs. A transient decrease in gas-phase H_2O in late January below 550 K indicates the very brief period with water ice formation described by *Jiménez et al*. [2006], as well as the intrusion of extra-vortex air described by *Schoeberl et al*. [2006]. The overall morphology of SD-WACCM gas-phase HNO_3 is qualitatively similar to that of MLS, as shown in Figures 2p–2r. Quantitatively, however, these comparisons are less favorable than the H_2O comparisons. Below 550 K, SD-WACCM exhibits a high bias in December through February, with short-term differences up to +30%. In late January and mid February below ~500 K, both SD-WACCM and MLS show transient decreases in HNO_3 separated by a brief increase, but the variations are less pronounced in SD-WACCM. The low HNO_3 mixing ratios at these times and altitudes likely represent pulses of increased heterogeneous processing in which gas-phase HNO_3 is taken up by PSCs. These pulses coincide with low temperatures shown in Figures 2a and 2b.

[34] Figure 7 shows MLS and SD-WACCM partial columns of gas-phase HNO_3 from 400 K to 700 K. Also shown is the partial column of SD-WACCM condensed-phase HNO_3 and the MLS temperature at 550 K. In contrast to Figure 2, Figure 7 shows column densities, which are vertically integrated quantities. The lower isentropic levels of Figure 2 are weighted more heavily than higher levels because the atmospheric density decreases with altitude. Therefore some of the SD-WACCM minus MLS differences that are apparent in Figure 2 are not evident in Figure 7. Partial columns of HNO_3 are discussed here as opposed to volume mixing ratios in order to show the total transient exchange between the gas phase and the condensed phase in the lower stratosphere. This exchange is largely controlled by temperature inside the vortex, but the resulting profiles of gas- and condensed-phase HNO_3 inside the vortex are also determined by the amount of descent. Therefore, comparisons of mixing ratios and temperatures on individual isentropic levels do not necessarily provide a self-consistent explanation of physical and chemical processes. For instance, after PSCs are formed by gas-phase HNO_3 uptake, they will descend. This means that atmospheric temperatures at a lower isentropic level are not necessarily well correlated with condensed-phase HNO_3 that originated at higher altitudes. A similar argument can be made for gas-phase HNO_3 because of evaporation of PSCs due to higher temperature at lower levels. Thus, Figure 7 adds to the information that can in part be inferred from Figure 2 by showing partial columns rather than individual isentropic levels. The time series of gas-phase HNO_3 partial columns (Figure 7) for SD-WACCM and MLS show very similar relative variations. However, the absolute difference is consistent with the model's overestimate of gas-phase HNO_3 after mid December that is shown in Figure 2r. The late January and mid February episodic decreases in the partial column of gas-phase HNO_3 are accompanied by increases in condensed phase HNO_3 in SD-WACCM and decreases in temperature, suggesting that those transient declines in gas-phase HNO_3 were indeed caused by PSC uptake. Similarly, the strong anti-correlation from mid December through late February between SD-WACCM condensed-phase HNO_3 and gas-phase HNO_3 from both SD-WACCM and MLS suggests that many of the observed, short-term fluctuations in HNO_3 were caused by ongoing exchanges between the gas and condensed phases.

[35] Also shown in Figure 7 is the total (sum of gas-phase and condensed-phase) HNO_3 simulated by SD-WACCM. The simulated total HNO_3 declines gradually by ~40% throughout January and February, leveling off in March. This apparent loss of HNO_3 is due to diabatic descent and sedimentation of NAT particles to isentropic levels below 400 K, which is evident from Figure 2q especially in late December through January. Transport from higher altitudes will also decrease the HNO_3 partial column, but not enough to account for the apparent loss shown in Figure 7. Also, isentropic mixing across the vortex edge reduces gas-phase HNO_3 inside the vortex because mixing ratios outside are generally lower between 400 K and 700 K (not shown). There is very little signature in the total HNO_3 of the transient pulse discussed above, while it is noticeable in the individual condensed-phase and gas-phase time series. This is further confirmation that the observed, short-term HNO_3 variations are simply indicative of an exchange of material between the gas and condensed phases. By the end of February, SD-WACCM indicates that no more condensed-phase HNO_3 is present; it is likewise reasonable to assume that at this time the MLS observations of gas-phase HNO_3 are about equal to total HNO_3 especially since the polar vortex average temperature is warm enough for most of the condensed-phase HNO_3 to evaporate. The model was initialized with MLS HNO_3, yet the total HNO_3 is higher in SD-WACCM than in MLS in March. This reflects a small (<10%) underestimate by SD-WACCM of HNO_3 removal from the 400 K to 700 K vortex region. With the observations shown, however, it is not possible to quantify errors in the

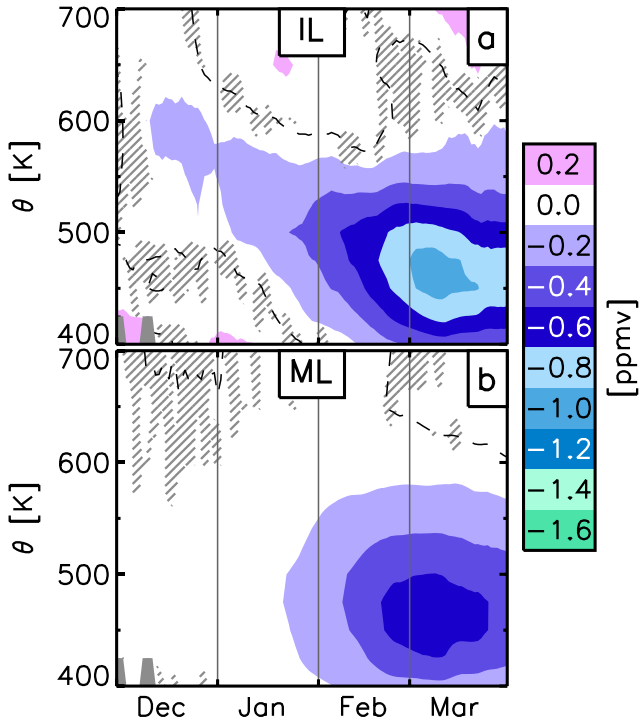

Figure 8. Evolution of the O_3 loss profile using the pseudo-passive subtraction technique for the inferred loss (MLS O_3 – SD-WACCM ppO_3;a) and for the modeled loss (SD-WACCM O_3 – SD-WACCM ppO_3;b). Both panels show O_3 loss due to heterogeneously activated halogens only. Hatched areas denote insignificant O_3 loss (95% confidence level). Black dashed lines denote the zero O_3 loss contour.

simulated uptake of HNO_3 by PSCs, in the estimation of PSC sedimentation, or in transport/mixing.

4. Discussion

[36] The differences between SD-WACCM and MLS described in the previous section clearly have implications for quantifying chemical O_3 loss, as mentioned above. This section shows O_3 loss calculations based on the pseudo-passive subtraction technique [*Singleton et al.*, 2005]. For the temperature regime observed in the 2004–2005 Arctic vortex, reaction rates for the reaction of $ClONO_2$ and HCl on aerosol surfaces are especially sensitive to small temperature variations [e.g., *Lowe and MacKenzie*, 2008]. Hence, this section also discusses the temperature sensitivity of the O_3 loss simulations.

4.1. Ozone Loss

[37] To calculate O_3 loss using the pseudo-passive subtraction technique, two simulations are run [*Singleton et al.*, 2005]. In the first, O_3 is fully active; it is allowed to participate in all relevant reactions, and active halogen species are produced via standard heterogeneous chemistry. This is the run to which MLS measurements have been compared in the previous section. In the second simulation, O_3 is treated as a pseudo-passive tracer. In this case O_3 is allowed to participate in all relevant reactions, but no halogen-containing heterogeneous chemistry is allowed, so halogens are not activated. The heterogeneous reaction of nitrogen pentoxide (N_2O_5) with H_2O is allowed, in order to maintain the correct reactive odd nitrogen (NO_y) partitioning. In many of the previous passive subtraction studies [e.g., *Manney et al.*, 1995; *Deniel et al.*, 1998; *Manney et al.*, 2003; *Grooß and Müller*, 2007; *Singleton et al.*, 2007; *Jackson and Orsolini*, 2008], O_3 has been treated as a fully passive tracer that is not allowed to participate in any chemical reactions. Because the lack of chemistry outside the vortex can lead to large errors in the amount of O_3 transported into the vortex, a fully passive tracer simulation was not employed in the work described here. In the pseudo-passive subtraction approach, the O_3 loss inferred from the observations ("IL" for "Inferred Loss") is defined as the observed O_3 minus the simulated, pseudo-passive O_3. This difference quantifies the O_3 loss catalyzed by halogens activated by heterogeneous chemistry. In the potential temperature regime of 400 to 600 K, halogens are the dominant O_3 loss catalyst. Since NO_x is the dominant O_3 loss catalyst above 600 K, the O_3 loss presented here is representative of the total chemical O_3 loss in the lower stratosphere. Analogous to the IL, the modeled ozone loss ("ML" for "Modeled Loss") is defined as the simulated, fully active O_3 minus the simulated, pseudo-passive O_3. Thus, the differences between the red (black) and solid blue curves in Figure 3 represent the ML (IL) using MLS and SD-WACCM results at 450 K.

[38] Figure 8 shows contour plots of the vortex average inferred and modeled O_3 loss from 400–700 K throughout the winter. Note that since the inferred loss is simply the measured O_3 minus the pseudo-passive O_3, and the modeled loss is the simulated (active) O_3 minus the pseudo-passive O_3, the difference between the two panels in Figure 8 (not shown) is equal to the difference between MLS O_3 and SD-WACCM O_3 in Figure 2f. As expected, both the inferred and modeled loss maximize in early March before the final warming. The altitude of the peak loss, both inferred from the observations and in the model, is at about 475 K. The O_3 loss inferred from the observations is larger throughout January–March, however, with a maximum inferred loss of about 1.0 ppmv and maximum modeled loss of only ~0.6 ppmv. A more conservative choice of the polar vortex edge definition leads to slightly higher O_3 loss; e.g., an sPV threshold of 1.6×10^{-4} s^{-1} corresponds to a maximum of 1.1 ppmv for vortex-averaged O_3 loss.

[39] Since polar vortex averages cannot be used to quantify local peaks in O_3 loss, Figure 9 shows the spatial distribution of inferred O_3 loss on the 475 K isentropic surface for 7 March 2005. This date and altitude were chosen to coincide with the greatest O_3 loss found in Figure 8. Note that for Figure 9 the whole day of MLS observations and sampled SD-WACCM output were gridded as described in section 2. The superimposed polar vortex edge is from 12 UTC. The distribution of O_3 loss inside the polar vortex is not homogeneous: local inferred loss due to heterogeneous chemistry ranges from 0.4 to 1.6 ppmv. This is consistent with findings of local O_3 loss maxima by *Manney et al.* [2006]. Figure 9 also shows O_3 loss outside the polar vortex, which likely arises from mixing across the polar vortex edge: an air parcel can experience O_3 loss inside the polar vortex and then be transported outside the polar vortex. Another possibility, in which an air parcel containing Cl_2 or activated Cl is transported outside the polar vortex, where O_3 loss then occurs,

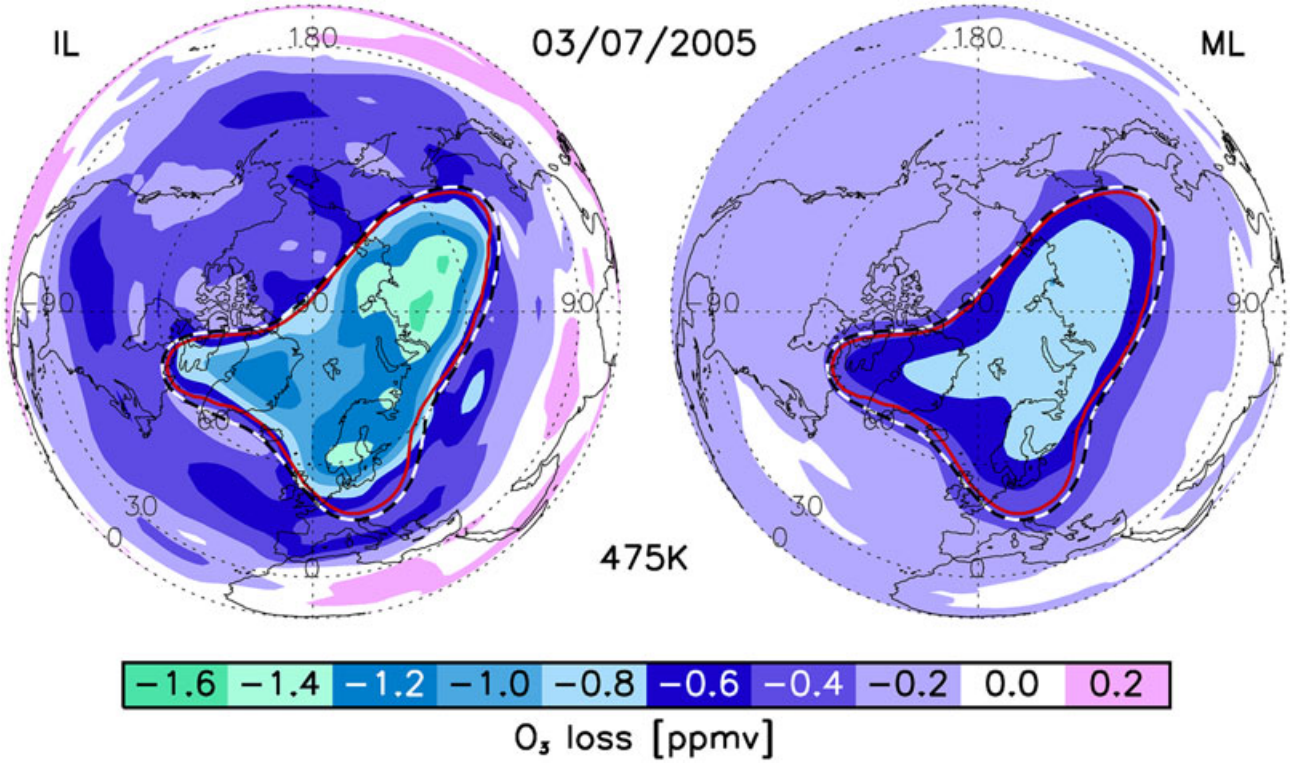

Figure 9. Spatial distribution of inferred O_3 loss (MLS O_3 − SD-WACCM ppO_3; left) and modeled O_3 loss (SD-WACCM O_3 − SD-WACCM ppO_3; right) at 475 K on 7 March 2005. The white/black dashed contour denotes the polar vortex edge as defined by an sPV threshold of 1.4×10^{-4} s^{-1}. The red contour line denotes the polar vortex edge using a 1.6×10^{-4} s^{-1} sPV threshold.

is rather unlikely due to efficient Cl deactivation outside the polar vortex [*Douglass et al.*, 1991; *Lee et al.*, 2002].

[40] As explained above, the most likely factors contributing to the differences between the inferred and modeled O_3 loss are too much mixing across the vortex edge and from the edge into the vortex core later in the winter, as well as too little halogen activation. In the absence of chemical O_3 loss, lower stratospheric O_3 mixing ratios outside the vortex would be lower than inside in late winter because of more descent inside the vortex. Too much mixing will therefore cause the simulated pseudo-passive O_3 in the lower stratospheric vortex to be underestimated; thus subtracting it from the observations will result in too little inferred loss. Even though our mixing errors contribute a negative bias to the simulated O_3 in the lower stratosphere late in the winter, the simulated, fully active O_3 mixing ratios are clearly too high (e.g., Figure 2f). Thus we conclude that even if mixing were simulated accurately, the HCl comparisons in late February suggest that SD-WACCM would underestimate chemical loss because of too little halogen activation. Indeed, the mixing errors are masking some of the halogen activation error that leads to too little simulated chemical loss.

4.2. Temperature Sensitivity

[41] Temperatures inside the polar vortex drop sufficiently low for STS and NAT particle formation in the second half of December and January [*Lowe and MacKenzie*, 2008]. In addition, localized temperatures are sometimes sufficiently low for small scale water ice particle formation [*Jiménez et al.*, 2006; *Lowe and MacKenzie*, 2008]. The temperature differences between MLS and SD-WACCM that are shown in Figure 2c are significant in the context of PSC formation probabilities and heterogeneous reaction rates. Thus in order to quantify the sensitivity of the O_3 loss calculations to temperature variability and possible temperature errors, we repeated the full chemistry O_3 simulation with a temperature bias of −1.5 K for the uptake reaction coefficients for all STS reactions [*Lowe and MacKenzie*, 2008; *Shi et al.*, 2001]. Also affected by the temperature bias is the parameterization of SAD formed by STS and NAT particles, as well as the HCl solubility. The choice of −1.5 K as a temperature modification for the heterogeneous chemistry in WACCM is justified by the discrepancies between MLS and SD-WACCM/GEOS5 temperature as discussed in section 3.1 and shown in Figure 2c at ~450 K. The temperature modification also falls in the range of known biases in MLS temperature of −2 to +1 K for isentropic levels between 400 and 700 K with a precision of ±0.6 to ±0.8 K [*Livesey et al.*, 2011]. In order to keep modeled dynamics consistent, the temperature bias is not applied in general but only to reaction coefficients and parameterizations in the heterogeneous chemistry module, as well as the HCl solubility in SD-WACCM.

[42] Figure 10 shows the same comparison as done in Figure 2 but applying a −1.5 K temperature bias to heterogeneous processing only. Figures 10b and 10c show this modified temperature. Observed and modeled O_3 agree to within 0.2 ppmv. In addition, the initial high O_3 bias that descends throughout the season, as explained in section 3.2, remains at a nearly constant value of ~0.1 ppmv.

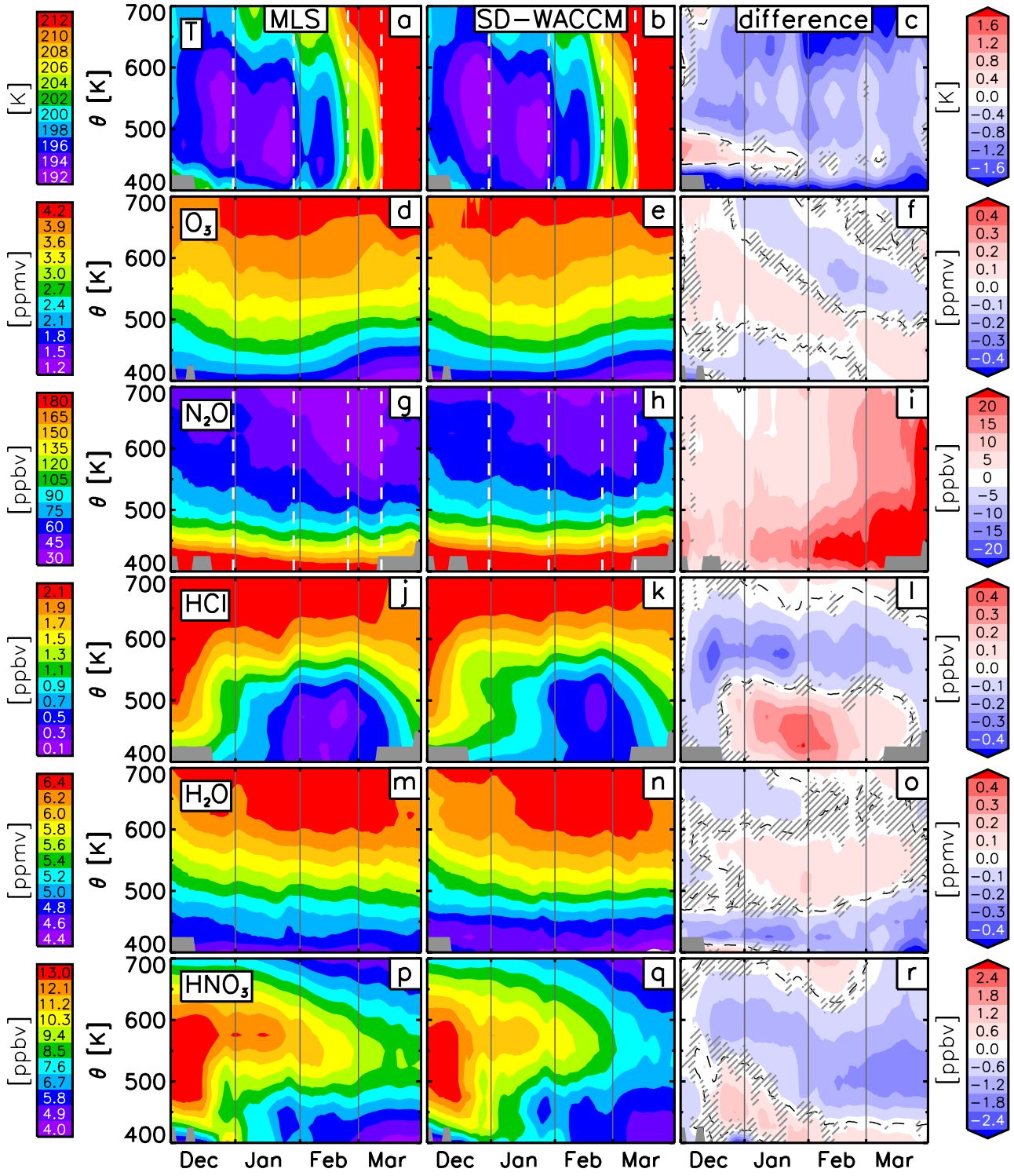

Figure 10. Same as Figure 2, but for SD-WACCM simulation using a −1.5 K temperature bias for heterogeneous chemistry reactions (see text).

Figure 4 shows that an overestimate in mixing across the vortex edge does not significantly increase O_3 inside the polar vortex below 500 K, since the cross-edge O_3 gradient in late winter is small. As a tracer N_2O is not significantly changed by the temperature bias. In general, more HCl is heterogeneously processed with the −1.5 K bias, as can be seen from the fact that the SD-WACCM minus MLS differences are smaller (less positive) with the −1.5 K bias. This is also supported by an increase in ClO (Figure 6, right), improving the averaged underestimate by SD-WACCM from ~34% without the temperature bias to ~19% with the temperature bias. Modeled HCl condensation with the temperature bias does not exceed a polar vortex average of 32 pptv in late January below 500 K (not shown),

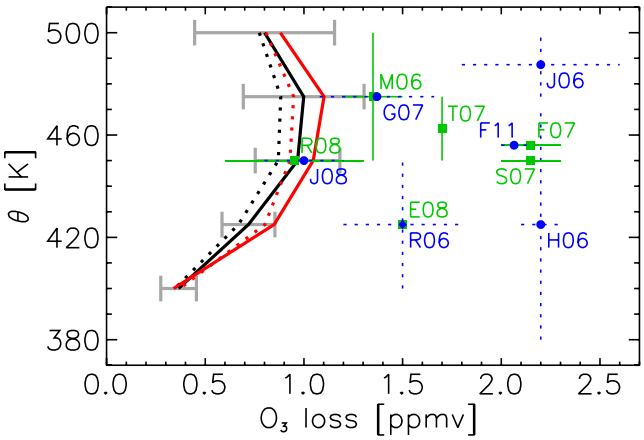

Figure 11. Comparison of our inferred (modeled) O_3 loss results (absolute values) shown as solid (dotted) line, using sPV thresholds of 1.4×10^{-4} s^{-1} (black) and 1.6×10^{-4} s^{-1} (red) as the vortex edge definition, with previous research listed in section 1: *Manney et al.* [2006] (M06); *Jin et al.* [2006b] (J06); *Rex et al.* [2006] (R06); *von Hobe et al.* [2006] (H06); *Feng et al.* [2007] (F07); *Grooß and Müller* [2007] (G07); *Singleton et al.* [2007] (S07); *Tsvetkova et al.* [2007] (T07); *El Amraoui et al.* [2008] (E08); *Jackson and Orsolini* [2008] (J08); *Rösevall et al.* [2008] (R08); and *Feng et al.* [2011] (F11). Horizontal and vertical lines show the O_3 loss range and the altitude range over which it was quantified. Blue and green colors as well as linestyles and symbols were chosen for better legibility and do not have any further meaning. Also shown are standard deviations of inferred O_3 loss results using an sPV threshold of 1.4×10^{-4} s^{-1} (gray).

which corresponds to a maximum of ~3.5% of total HCl in the condensed phase. But the late onset of heterogeneous processing, likely due to the $ClONO_2$ discrepancy and/or too little condensation of HCl as suggested in section 3.4, is still evident. Note that below 500 K, applying the −1.5 K bias brought the simulated and observed HCl into better agreement. There is a ≤0.35 ppmv low bias in SD-WACCM H_2O relative to MLS (Figure 10o) in the region where there is a remaining high bias in HCl (Figures 2 and 10), i.e., H_2O mixing ratios are independent of the temperature bias. This coupled with the uncertainty in the laboratory data [*Wegner et al.*, 2012b] used in the parameterization of HCl condensation could help explain the model high bias in HCl below 500 K. Above 500 K, however, the simulated HCl is now significantly too low. This makes sense since the temperature bias was chosen based on the 450 K level as described previously. Figures 10 and 7 show improvement of modeled gas-phase HNO_3, especially from mid January to the end of the season. From the improvement of the above-described related diagnostics, we conclude that with the temperature bias the heterogeneous processing is represented more realistically in the model.

[43] Figure 3 shows the effect of a 1.5 K temperature decrease on O_3 (dashed, red curve). The 1.5 K negative bias improves the agreement with observations from MLS (black curve) in February and March. When the temperature bias is applied, the maximum of the polar vortex averaged ML changes from 0.6 ppmv (shown in Figure 8b) to 1.0 ppmv (can be inferred from Figure 3, 7 March), which matches the IL. We conclude, therefore, that the parameterization of PSC microphysics in WACCM and the partitioning between NAT and STS in particular is improved as described by *Wegner et al.* [2012a]. *Lowe and MacKenzie* [2008] concluded that a sufficiently efficient and accurate parameterization of PSC microphysics and chemistry was not yet available for global chemistry climate models such as WACCM at that time. *Feng et al.* [2011] used the SLIMCAT 3-D chemical transport model coupled to a detailed microphysical model to study the 2004–2005 Arctic winter. Their simulations of denitrification and ozone compared well with MLS observations, leading them to conclude, in agreement with *Lowe and MacKenzie* [2008], that robust simulations of Arctic O_3 loss in chemistry climate models might require a full microphysical treatment. Our results show that simulations using the improved WACCM PSC parameterization are sufficiently accurate to warrant its use in order to conserve computational resources.

5. Summary and Conclusions

[44] The SD-WACCM simulations of O_3 inside the polar vortex in the Arctic winter of 2004–2005 generally compare well with O_3 observed by MLS. Agreement is within ~10%, indicating that SD-WACCM is a useful tool for investigating polar O_3 loss. However, there is a persistent high bias in SD-WACCM O_3 in the O_3 loss region below 550 K that is likely caused by deficiencies in the initialization procedure for O_3 (+0.1 ppmv) and too little heterogeneous processing (+0.3 ppmv). SD-WACCM simulations are most likely deficient in $ClONO_2$ in early winter, so that even in the presence of significant aerosol surface area, the reaction of HCl with $ClONO_2$ is too slow. The reason for the underestimate of $ClONO_2$ is not yet understood. Also the condensation of gas-phase HCl is likely underestimated due to an underestimate in ambient water vapor and an overestimate in temperature. SD-WACCM slightly overestimates isentropic mixing across the polar vortex edge and between the outer and inner regions of the vortex; descent inside the vortex is well simulated.

[45] Polar vortex average chemical O_3 loss was estimated to be 1.0 ppmv for the 2004–2005 Arctic winter using the pseudo-passive subtraction technique, with peak localized losses as high as 1.6 ppmv. Figure 11 compares absolute values of our vortex average results with previous findings based on various techniques that were briefly explained in section 1. O_3 loss estimates presented here are on the low end of the range of previous results. Vortex edge definitions used in the studies shown in Figure 11, however, were more conservative and thus emphasize O_3 loss in the vortex core more than in this study. A more conservative vortex edge definition is shown in Figure 9 as the red line and corresponding vortex averaged O_3 loss results are depicted by the red profile in Figure 11. The temperature sensitivity study in section 4.2 shows that the modeled evolution of O_3 agrees better with observations when a temperature bias of −1.5 K is imposed on heterogeneous chemistry reactions and SAD formation. In this case, only the high bias in SD-WACCM O_3 of ~0.1 ppmv that is attributed to the initialization procedure remains. Imposing such a temperature bias, however, does not resolve the late onset of HCl depletion,

which is likely due to a $ClONO_2$ deficiency and/or an underestimate of HCl condensation. In order to investigate the $ClONO_2$ deficiency, an in-depth analysis as presented here is planned for several winter seasons in which a better temporal coverage of $ClONO_2$ observations is available. Such an analysis also evaluates the interannual variability simulated by WACCM that could not be investigated in this study. Further work is required to more accurately simulate both isentropic mixing across the vortex edge as well as heterogeneous chemistry in WACCM.

[46] In conclusion, we have shown through comprehensive model-measurement comparisons that SD-WACCM reliably simulates most ozone related processes in the Arctic winter of 2004–2005, but questions remain regarding processes involving chlorine chemistry. Since models differ in, e.g., their parameterizations of various processes, the results of this study cannot be extrapolated in order to draw general conclusions about other CCMs and CTMs. Thus similar in-depth analyses and model/measurement comparisons or model inter-comparisons, e.g., the SPARC CCMVal Report [*Eyring et al*., 2010], are necessary to assess other individual CCMs and CTMs.

[47] **Acknowledgments.** We thank C.S. Singleton for helpful discussions. M.B. and C.E.R. were funded by JPL/NASA grant 1350080 and NSF award AGS 1135432. The SD-WACCM simulations were carried out at NCAR. NCAR is sponsored by the National Science Foundation. Work at the Jet Propulsion Laboratory, California Institute of Technology, was done under contract with the National Aeronautics and Space Administration.

References

Akiyoshi, H., Y., Yamashita, K., Sakamoto, L. B., Zhou, and T. Imamura (2010), Recovery of stratospheric ozone in calculations by the Center for Climate System Research/National Institute for Environmental Studies chemistry-climate model under the CCMVal-REF2 scenario and a no-climate-change run, *J. Geophys. Res.*, *115*, D19301, doi:10.1029/2009JD012683.

Blum, U., F., Khosrawi, G., Baumgarten, K., Stebel, R., Müller, and K. H. Fricke (2006), Simultaneous lidar observations of a polar stratospheric cloud on the east and west sides of the Scandinavian mountains and microphysical box model simulations, *Ann. Geophys.*, *24*, 3267–3277, doi:10.5194/angeo-24-3267-2006.

Brasseur, G. P., D. A., Hauglustaine, S., Walters, P. J., Rasch, J.-F., Muller, C., Granier, and X.-X. Tie (1998), MOZART, a global chemical transport model for ozone and related chemical tracers 1: Model description, *J. Geophys. Res.-Atmos.*, *103*, 28265–28289.

Brasseur, G. and S. Solomon (2005), *Aeronomy of the Middle Atmosphere—Chemistry and Physics of the Stratosphere and Mesosphere*, Springer, Dordrecht, Netherlands.

Collins, W. D., et al. (2006), The formulation and atmospheric simulation of the community atmosphere model version 3 (CAM3), *J. Climate*, *19*, 2144–2161, doi:10.1175/JCLI3760.1.

Deniel, C., R. M., Bevilacqua, J. P., Pommereau, and F. Lefèvre (1998), Arctic chemical ozone depletion during the 1994–1995 winter deduced from POAM II satellite observations and the REPROBUS three-dimensional model, *J. Geophys. Res.*, *D15*, 19, 231–19, 244.

Dibb, J. E., E., Scheuer, M., Avery, J., Plant, and G. Sachse (2006), In situ evidence for renitrification in the Arctic lower stratosphere during the polar Aura validation experiment (PAVE), *Geophys. Res. Lett.*, *33*, L12815, doi:10.1029/2006GL026243.

Douglass, A. R., R. B., Rood, J. A., Kaye, R. S., Stolarski, D. J., Allen, and E. M. Larson (1991), The influence of polar heterogeneous processes on reactive chlorine at middle latitudes: Three dimensional model implications, *Geophys. Res. Lett.*, *18*(1), 25–28, doi:10.1029/90GL02601.

Dowdy, S., S., Wearden, and D. Chilko (2004), *Statistics for Research—Third Edition*, Wiley, Hoboken, New Jersey, USA, doi:10.1002/0471477435.

Drdla, K. and R. Müller (2012), Temperature thresholds for chlorine activation and ozone loss in the polar stratosphere, *Ann. Geophys.*, *30*, 1055–1073, doi:10.5194/angeo-30-1055-2012.

Dunkerton, T. and D. Delisi (1986), Evolution of potential vorticity in the winter stratosphere of January-February 1979, *J. Geophys. Res.*, *91*, 1199–1208.

El Amraoui, L., N., Semane, V.-H., Peuch, and M. L. Santee (2008), Investigation of dynamical processes in the polar stratospheric vortex during the unusually cold winter 2004/2005, *Geophys. Res. Lett.*, *35*, L03803, doi:10.1029/2007GL031251.

Emmons, L. K., et al. (2010), Description and evaluation of the Model for Ozone and Related chemical Tracers, version 4 (MOZART-4), *Geosci. Model Dev.*, *3*, 43–67, 2010.

Esler, J. and D. Waugh (2002), A method for estimating the extent of denitrification of Arctic polar vortex air from tracer-tracer scatter plots, *J. Geophys. Res.*, *107*, doi:10.1029/2001JD001071.

Eyring, V., T. G. Shepherd, and D. W. Waugh (Eds), (2010), SPARC report on the evaluation of Chemistry-Climate Models, *SPARC Report No*. *5*, WCRP-132, WMO/TD-No. 1526.

Feng, W., M. P. Chipperfield, S. Davies, P. von der Gathen, E. Kyroe, C. M. Volk, A. Ulanovsky, and G. Belyaev (2007), Large chemical ozone loss in 2004/2005 Arctic winter/spring, *Geophys. Res. Lett.*, *34*, L09803, doi:10.1029/2006GL029098.

Feng, W., et al. (2011), Modelling the effect of denitrification on polar ozone depletion for the Arctic winter 2004/2005, *Atmos. Chem. Phys.*, *11*, 6559–6573, 2011, doi:10.5194/acp-11-6559-2011.

Grooß, J.-U., and R. Müller (2007), Simulation of ozone loss in Arctic winter 2004/2005, *Geophys. Res. Lett.*, *34*, L05804, doi:10.1029/2006GL028901.

Hauglustaine, D. A., G. P., Brasseur, S., Walters, P. J., Rasch, Müller, J.-F., L. K., Emmons, and M. A. Carroll (1998), MOZART: A global chemical transport model for ozone and related chemical tracers: 2. Model results and evaluation, *J. Geophys. Res.*, *103*, 28291–28335.

Hoppel, K., et al. (2002), POAM III observations of arctic ozone loss for the 1999/2000 winter, *J. Geophys. Res.*, *107*, doi:10.1029/2001JD000476.

Horowitz, L. W., et al. (2003), A global simulation of tropospheric ozone and related tracers: Description and evaluation of MOZART, version 2, *J. Geophys. Res.*, *108*(D24), 4784, doi:10.1029/2002JD002853.

Jackson, D. R. and Y. J. Orsolini (2008), Estimation of Arctic ozone loss in winter 2004/05 based on assimilation of EOS MLS and SBUV/2 observations, *Q. J. R. Meteorol. Soc.*, *134*, 1833–1841, doi:10.1002/qj.316.

Jiménez, C., H. C. Pumphrey, I. A. MacKenzie, G. L. Manney, M. L. Santee, M. J. Schwartz, R. S. Harwood, and J. W. Waters (2006), EOS MLS observations of dehydration in the 2004–2005 polar winters, *Geophys. Res. Lett.*, *33*, L16806, doi:10.1029/2006GL025926.

Jin, J. J., et al. (2006a), Denitrification in the Arctic winter 2004/2005: Observations from ACE-FTS, *Geophys. Res. Lett.*, *33*, L19814, doi:10.1029/2006GL027687.

Jin, J. J., et al. (2006b), Severe Arctic ozone loss in the winter 2004/2005: Observations from ACE-FTS, *Geophys. Res. Lett.*, *33*, L15801, doi:10.1029/2006GL026752.

Kinnison, D. E., et al. (2007), Sensitivity of chemical tracers to meteorological parameters in the MOZART-3 chemical transport model, *J. Geophys. Res.*, *112*, D20302, doi:10.1029/2006JD007879.

Kleinböhl, A., H., Bremer, H., Küllmann, J., Kuttippurath, E. V., Browell, T., Canty, R. J., Salawitch, G. C., Toon, and J. Notholt (2005), Denitrification in the Arctic midwinter 2004/2005 observed by airborne submillimeter radiometry, *Geophys. Res. Lett.*, *32*, L19811, doi:10.1029/2005GL023408.

Knuth, D. E. (1992), *Axioms and Hulls*, Springer-Verlag, Berlin/Heidelberg, Germany.

Kunz, A., L., Pan, P., Konopka, D., Kinnison, and S. Tilmes (2011), Chemical and dynamical discontinuity at the extratropical tropopause based on START08 and WACCM analysis, *J. Geophys. Res.*, *116*, D24302, doi:10.1029/2011JD016686.

Lamarque, J.-F., et al. (2012), CAM-chem: Description and evaluation of interactive atmospheric chemistry in the Community Earth System Model, *Geosci. Model Dev.*, *5*, 369–411, doi:10.5194/gmd-5-369-2012.

Lee, A. M., Jones, R. L., Kilbane-Dawe, I., and J. A. Pyle (2002), Diagnosing ozone loss in the extratropical lower stratosphere, *J. Geophys. Res.*, *107*, 4110, doi:10.1029/2001JD000538.

Lin, S.-J. and R. B. Rood (1996), Multidimensional flux-form semi-Lagrangian transport schemes, *Mon. Wea. Rev.*, *124*, 2046–2070, doi:10.1175/1520-0493(1996)124 < 2046:MFFSLT > 2.0.CO;2.

Lin, S.-J. (2004), A "vertically Lagrangian" finite-volume dynamical core for global models, *Mon. Wea. Rev.*, *132*, 2293–2307, doi:10.1175/1520-0493(2004)132 < 2293:AVLFDC > 2.0.CO;2.

Livesey, N. J., et al. (2011), Earth Observing System (EOS) Aura Microwave Limb Sounder (MLS) Version 3.3 Level 2 data quality and description document, Jet Propulsion Laboratory, California Institute of Technology, Pasadena, California.

Loewenstein, M., J. R., Podolske, K. R., Chan, and S. E. Strahan (1990), N_2O as a dynamical tracer in the Arctic vortex, *Geophys. Res. Lett.*, *17*(4), 477–480, doi:10.1029/GL017i004p00477.

Lowe, D. and A. R. MacKenzie (2008), Polar stratospheric cloud microphysics and chemistry, *J. Atmos. Sol.-Terr. Phy.*, *70*, 13–40, doi:10.1016/j.jastp.2007.09.011.

Manney, G. L., et al. (1995), Lagrangian transport calculations using UARS data. Part I: Passive tracers, *J. Atmos. Sci.*, *52*(17), 3049–3068.

Manney, G. L., L., Froidevaux, M. L., Santee, N. J., Livesey, J. L., Sabutis, and J. W. Waters (2003), Variability of ozone loss during Arctic winter (1991–2000) estimated from UARS Microwave Limb Sounder measurements, *J. Geophys. Res.*, *108*(D4), 4149, doi:10.1029/2002JD002634.

Manney, G. L., M. L., Santee, L., Froidevaux, K., Hoppel, N. J., Livesey, and J. W. Waters (2006), EOS MLS observations of ozone loss in the 2004–2005 Arctic winter, *Geophys. Res. Lett.*, *33*, L04802, doi:10.1029/2005GL024494.

Michelsen, H. A., et al. (1998), Correlations of stratospheric abundances of NO_y, O_3, N_2O, and CH_4 derived from ATMOS measurements, *J. Geophys. Res.*, *103*, 28347– 28359.

Pitts, M. C., L. R., Poole, and L. W. Thomason (2009), CALIPSO polar stratospheric cloud observations: Second-generation detection algorithm and composition discrimination, *Atmos. Chem. Phys.*, *9*, 7577–7589, doi:10.5194/acp-9-7577-2009.

Portmann, R. W., S., Solomon, R. R., Garcia, L. W., Thomason, L. R., Poole, and M. P. McCormick (1996), Role of aerosol variations in anthropogenic ozone depletion in the polar regions, *J. Geophys. Res.*, *101*(D17), 22991–23006, doi:10.1029/96JD02608.

Proffitt, M. H., S., Solomon, and M. Loewenstein (1992), Comparison of 2-D model simulations of ozone and nitrous oxide at high latitudes with stratospheric measurements, *J. Geophys. Res.*, *97*, 939–944.

Reinecker, M. M., et al. (2008), The GEOS-5 data assimilation system—Documentation of versions 5.0.1 and 5.1.0, *Tech. Rep. NASA/TM-2007-104606*, Vol. 27, NASA GSFC.

Rex, M., et al. (1999), Chemical ozone loss in the Arctic winter 1994/95 as determined by the match technique, *J. Atmos. Chem.*, *32*, 35–59.

Rex, M., R. J. Salawitch, P. von der Gathen, N. R. P. Harris, M. P. Chipperfield, and B. Naujokat (2004), Arctic ozone loss and climate change, *Geophys. Res. Lett.*, *31*, doi:10.1029/2003GL018844.

Rex, M., et al. (2006), Arctic winter 2005: Implications for stratospheric ozone loss and climate change, *Geophys. Res. Lett.*, *33*, L23808, doi:10.1029/2006GL026731.

Richter, J. H., F. Sassi, and R. R. Garcia (2010), Toward a physically based gravity wave source parameterization in a general circulation model, *J. Atmos. Sci.*, *67*, doi:10.1175/2009JAS3112.1.

Roble, R. G., and E. C. Ridley (1987), An auroral model for the NCAR thermospheric general circulation model (TGCM), *Ann. Geophys.*, *87*, 369–382.

Rösevall, J., D., Murtagh, J., Urban, W., Feng, P., Eriksson, and S. Brohede, (2008), A study of ozone depletion in the 2004/2005 Arctic winter based on data from Odin/SMR and Aura/MLS, *J. Geophys. Res.*, *113*, 20, doi:10.1029/2007JD009560.

Salawitch, R. J., et al. (2010), A new interpretation of total column BrO during Arctic spring, *Geophys. Res. Lett.*, *37*, L21805, doi:10.1029/2010GL043798.

Santee, M. L., I. A., MacKenzie, G. L., Manney, M. P., Chipperfield, P. F., Bernath, K. A., Walker, C. D., Boone, L., Froidevaux, N. J., Livesey, and J. W. Waters (2008), A study of stratospheric chlorine partitioning based on new satellite measurements and modeling, *J. Geophys. Res.*, *113*, D12307, doi:10.1029/2007JD009057.

Schoeberl, M. R., et al. (2006), Chemical observations of a polar vortex intrusion, *J. Geophys. Res.*, *111*, D20306, doi:10.1029/2006JD007134.

Schwartz, M. J., et al. (2008), Validation of the Aura Microwave Limb Sounder temperature and geopotential height measurements, *J. Geophys. Res.*, *113*, D15S11, doi:10.1029/2007JD008783.

Shepherd, T. G. (2000), The middle atmosphere, *J. Atmos. Sol.-Terr. Phy.*, *62*, 1587–1601, doi:10.1016/S1364-6826(00)00114-0.

Shi, Q., J., Jayne, C., Kolb, D., Worsnop, and P. Davidovits (2001), Kinetic model for reaction of ClONO2 with H2O and HCl and HOCl with HCl in sulfuric acid solutions, *J. Geophys. Res.-Atmos.*, *106*, 24259–24274.

Singleton, C. S., C. E., Randall, M. P., Chipperfield, S., Davies, W., Feng, R. M., Bevilacqua, K. W., Hoppel, M. D., Fromm, G. L., Manney, and V. L. Harvey (2005), 2002–2003 Arctic ozone loss deduced from POAM III satellite observations and the SLIMCAT chemical transport model, *Atmos. Chem. Phys.*, *5*, 597–609, doi:10.5194/acp-5-597-2005.

Singleton, C. S., et al. (2007), Quantifying Arctic ozone loss during the 2004–2005 winter using satellite observations and a chemical transport model, *J. Geophys. Res.*, *112*. doi:10.1029/2006JD007463.

Solomon, S. (1999), Stratospheric ozone depletion: A review of concepts and history, *Rev. Geophys.*, *37*, 275–316.

Tilmes, S., R., Müller, J., Grooß, and J. Russell (2004), Ozone loss and chlorine activation in the Arctic winters 1991–2003 derived with the tracer-tracer correlations, *Atmos. Chem. Phys.*, *4*, 2181–2213.

Tilmes, S., D. E., Kinnison, R. R., Garcia, R., Salawitch, T., Canty, J., Lee-Taylor, S., Madronich, and K. Chance (2012), Impact of very short-lived halogens on stratospheric ozone abundance and UV radiation in a geo-engineered atmosphere, *Atmos. Chem. Phys.*, *12*, 10945–10955, doi:10.5194/acp-12-10945-2012.

Tsvetkova, N. D., V. A., Yushkov, A. N., Luk'yanov, V. M., Dorokhov, and H. Nakane (2007), Record-breaking chemical destruction of ozone in the Arctic during the winter of 2004/2005, *Izvestiya*, *Atmos. Oceanic Phys.*, *43*, 5, doi: 10.1134/S0001433807050076.

von Hobe, M., et al. (2006), Severe ozone depletion in the cold Arctic winter 2004–05, *Geophys. Res. Lett.*, *33*, L17815, doi:10.1029/2006GL026945.

Wegner, T., J.-U., Grooß, M., von Hobe, F., Stroh, O., Sumińska-Ebersoldt, C. M., Volk, E., Hösen, V., Mitev, G., Shur, and R. Müller (2012), Heterogeneous chlorine activation on stratospheric aerosols and clouds in the Arctic polar vortex, *Atmos. Chem. Phys.*, *12*, 11095–11106, doi:10.5194/acp-12-11095-2012, 2012.

Wilcoxon, F. (1945), Individual comparisons by ranking methods, *Biometrics Bull.*, *1*, 6, 80–83.

Wilks, D. S. (2006), Statistical methods in the atmospheric sciences, 2nd ed., *International Geophysics Series*, Volume *91*, Academic Press, San Diego.

World Meteorological Organization (2011), Scientific assessment of ozone depletion: 2010. Global Ozone Research and Monitoring Project - NO. 52, 516pp, World Meteorological Organization, Geneva, Switzerland.